A STANDARD LINEAR SOLID MODEL REPRESENTATION OF FREQUENCY-DEPENDENT ANISOTROPY DUE TO MULTIPLE SETS OF ALIGNED MESO-SCALE FRACTURES

QI HAO[1]* and QIAODENG HE[2]

[1] *China University of Petroleum, Qingdao, P.R. China.*
[2] *Jilin University, Changchun, P.R. China. Heqiaodeng@gmail.com*
* *Present address: NTNU, Trondheim, Norway. qi.hao@ntnu.no*

(Received October 9, 2012; revised version accepted March 2, 2013)

ABSTRACT

Hao, Q. and He, Q., 2013. A standard linear solid model representation of frequency-dependent anisotropy due to multiple sets of aligned meso-scale fractures. *Journal of Seismic Exploration*, 22: 169-182.

The effective medium theory developed by Chapman (2003) has been used to interpret the phenomena of frequency-dependent anisotropy in porous media with meso-scale fractures. However, until recently, no research has attempted to study the propagation of seismic waves in media with meso-scale fractures. Considering a large amount of expensive numerical computation using frequency-domain modelling approaches, the key is to obtain the time-domain explicit constitutive relationships for this model. In this paper, a standard linear solid (SLS) model is used to represent frequency-dependent anisotropy in media with two sets of aligned mesoscapic fractures. Meanwhile, we find that the order of the SLS model used to represent Chapman's model is no more than four. Consequently, two types of time-domain constitutive relationship are obtained by introducing auxiliary differential equations. Furthermore, based on the first-order velocity-stress wave equations, the time-domain numerical modelling can be applied to simulate the wave propagation in such media.

KEY WORDS: frequency-dependent anisotropy, numerical modeling, standard linear solid, fracture, finite-difference.

INTRODUCTION

Frequency-dependent anisotropy has been observed in porous media with one or multiple sets of aligned fractures. Chapman (2003) developed a model for the frequency dependence of the viscoelastic stiffness tensor for an equant-porosity medium. In this model, aligned meso-scale fractures are embedded in

0963-0651/13/$5.00

a porous medium, which includes micro-scale pores and micro-cracks. This model has been extended to account for two sets of meso-scale fracture with different orientations and connectivities (Chapman, 2009). Recently, Tillotson et al. (2011) demonstrated the validity of this model using laboratory experiments. The current application of this model has been focused on analysis of frequency-dependence of shear-wave splitting (Liu et al., 2003a, 2003b, 2006; Maultzsch et al., 2003, 2007; Liu, 2005; Al-Harrasi et al., 2011).

Until now, the characterization of seismic wave propagation in this model has not been studied. This is due to the complication of viscoelastic stiffness of this model. It is very difficult to directly apply frequency-domain modelling method to simulate seismic wave propagation in such a viscoelastic model, because the inversion of a large complex-valued sparse matrix has to be performed. This paper is aimed to explicitly represent Chapman's (2009) model using the standard linear solid model (SLS) and then apply time-domain numerical modelling methods, such as finite-difference and finite-element.

REVIEW OF CHAPMAN'S MODEL

Two kinds of scales have been considered in Chapman's (2009) model. One is the micro-scale pore, and the other is the meso-scale fracture. Generally, the viscoelastic stiffness can be written as

$$C_{ijkl} = C^0_{ijkl} - C^p_{ijkl} - \sum_{m=1}^{2} R^m_{ip} R^m_{jq} R^m_{kr} R^m_{ls} a^m_{pqrs} \quad , \tag{1}$$

where superscript 'p' indicates pore-related variables. Superscript '0' represents isotropic matrix (reference rock). Superscript 'm' represents the m-th set of fractures. C^0_{ijkl} denotes the elastic stiffness of reference isotropic rock. C^p_{ijkl} represents the stiffness correction for the presence of the pores. It can be written in standard tensor form as

$$C^p_{ijkl} = [d - (2/3)e]\delta_{ij}\delta_{kl} + e(\delta_{ik}\delta_{jl} + \delta_{il}\delta_{jk}) \quad , \tag{2}$$

where

$$d = \varphi^0_p\left[[(3\lambda+4\mu)/12\mu][\{(1-\upsilon)/(1+\upsilon)\}\sigma^5_{ll} - p^*] - (1/3)p^*\right] \quad , \tag{3}$$

$$e = \varphi^0_p 15\mu[(1 - \upsilon)/(7 + 5\upsilon)] \quad , \tag{4}$$

and φ^0_p is the pore porosity. p^* is the fluid pressure,

$$p^* = H^3_{ij}\sigma^5_{ij} \quad . \tag{5}$$

R^m_{ip} in eq. (1) is the rotation matrix which is obtained from the unit normal vector to the m-th fracture surface defined by angles θ_m and φ_m.

a^m_{pqrs} is the stiffness correction tensor for the m-th set of horizontal fractures in which the normal direction is parallel to the vertical axes. The non-zero components of a^m_{pqrs} are:

$$a^m_{11} = \varphi^0_m[(\lambda/\sigma^m_c)(\lambda - f^1_m) - f^1_m] \ , \tag{6}$$

$$a^m_{33} = \varphi^0_m[\{(\lambda + 2\mu)/\sigma^m_c\}(\lambda + 2\mu - f^2_m) - f^2_m] \ , \tag{7}$$

$$a^m_{12} = \varphi^0_m[(\lambda/\sigma^m_c)(2\lambda - f^3_m) - f^3_m] - \tfrac{1}{2}(a^m_{11} + a^m_{33}) \ , \tag{8}$$

$$a^m_{13} = \varphi^0_m[\{(\lambda + \mu)/\sigma^m_c\}(2\lambda + 2\mu - f^4_m) - f^4_m] - \tfrac{1}{2}(a^m_{11} + a^m_{33}) \ , \tag{9}$$

$$a^m_{55} = \varphi^0_m[4\mu(1 - \upsilon)/\{\pi(2 - \upsilon)r_m\}] \ , \tag{10}$$

$$a^m_{66} = \tfrac{1}{2}(a^m_{11} - a^m_{12}) \ . \tag{11}$$

In eq. (10), r_m is the aspect ratio of the m-th set of fracture, υ is the Poisson's ratio of the reference media. f^p_m (p = 1, 2, 3 and 4) in eqs. (6) to (9) can be represented as

$$f^p_m = H^m_{ij}R^m_{ia}R^m_{jb}\sigma^p_{ab} \ , \quad p = 1, 2, 3, 4 \ , \tag{12}$$

where the expression for H^m_{ij} is

$$H^m_{ij}(\omega) = S^m_{ij}(\omega) + F_m(\omega)H^3_{ij}(\omega) \ , \tag{13}$$

$$S^m_{ij}(\omega) = i\omega\tau_m n^m_i n^m_j/[(1 + i\omega\tau_m)(1 + K^m_c)] \ , \tag{14}$$

$$F_m(\omega) = 1/(1 + i\omega\tau_m) \ . \tag{15}$$

In eq. (14), n^m_i denotes the i-th component of the unit vector for the m-th set of fracture. τ_m denotes the corresponding relaxation time,

$$\tau_m = [8\ell(1 - \upsilon)(1 + K^m_c)/3\mu](\eta/k)a^m_f \ , \tag{16}$$

where ℓ has the meaning of a separation between the adjacent inter-granular voids. η and k represent the viscosity and permeability for the fluid in fractured rock, respectively. a^m_f denotes the radius of the m-th fracture. The expression for K^m_c reads

$$K^m_c = \pi\mu r_m/[2(1 - \upsilon)\kappa_f] \ . \tag{17}$$

In eq. (17), κ_f is the bulk modulus of fluid. Moreover, the expression for H^3_{ij} in eqs. (5) and (13) is

$$H^3_{ij} = \Big(\sum_{m=1}^{2} (\varphi^0_m/\sigma^m_c)[n^m_i n^m_j - (1+K^m_c)S^m_{ij}(\omega)] + (3\varphi^0_p/4\mu)[(1-\upsilon)/(1+\upsilon)]\delta_{ij} \Big) \Big/ \Big(\sum_{m=1}^{2} (\varphi^0_m/\sigma^m_c)(1 + K^m_c)F_m(\omega) + (3\varphi^0_p/4\mu)(1 + K_p) \Big) \quad . \tag{18}$$

$$K_p = 4\mu/3\kappa_f \quad . \tag{19}$$

SLS MODEL REPRESENTATION OF CHAPMAN'S MODEL

According to eqs. (1) to (19), we find that frequency-dependent terms in Chapman's model can be written in the form of a SLS model. Consequently, the viscoelastic stiffness (1) can also be written in the form of SLS models. In the following derivation, the subscript and superscript m are taken to be 1 and 2.

SLS model representation of H^3_{ij}

We assume that H^3_{ij} in eq. (18) can be written in the following form:

$$H^3_{ij} = \Lambda_{0ij} + [\Lambda_{1ij}/(1 + i\omega\tau_3)] + [\Lambda_{2ij}/(1 + i\omega\tau_4)] \quad . \tag{20}$$

Then we can determine those unknown variables in the above equation by fitting eq. (20) with eq. (18). Finally, coefficients Λ_{kij}, k = 0,1,2 are obtained,

$$\Lambda_{0ij} = \gamma_{0ij} \quad , \tag{21}$$

$$\Lambda_{1ij} = [e_2(\gamma_{1ij}-\gamma_{0ij})(\tau_2-\tau_3) + e_3(\gamma_{2ij}-\gamma_{0ij})(\tau_1-\tau_3)]/(\tau_4-\tau_3) \quad , \tag{22}$$

$$\Lambda_{2ij} = [e_2(\gamma_{1ij}-\gamma_{0ij})(\tau_4-\tau_2) + e_3(\gamma_{2ij}-\gamma_{0ij})(\tau_4-\tau_1)]/(\tau_4-\tau_3) \quad , \tag{23}$$

$$\tau_{3,4} = \{[e_1(\tau_1+\tau_2) + e_2\tau_2 + e_3\tau_1] \pm \sqrt{\Delta}\}/2 \quad , \tag{24}$$

$$\Delta = [e_1(\tau_1+\tau_2) + e_2\tau_2 + e_3\tau_1]^2 - 4e_1\tau_1\tau_2$$

$$= \tau_1^2(e_1 + e_3)^2 + \tau_2^2(e_1 + e_2)^2 + 2\tau_1\tau_2(e_2e_3 - e_1) \quad , \tag{25}$$

$$e_k = \beta_{k-1}/(\beta_0 + \beta_1 + \beta_2) \quad , \quad k = 1,2,3, \tag{26}$$

$$\gamma_{kij} = \alpha_{kij}/\beta_k \quad , \quad k = 0,1,2, \tag{27}$$

$$\alpha_{0ij} = (3\varphi_p^0/4\mu)[(1-\upsilon)/(1+\upsilon)]\delta_{ij} \ , \ \alpha_{1ij} = n_i^1 n_j^1(\varphi_1^0/\sigma_c^1) \ ,$$

$$\alpha_{2ij} = n_i^2 n_j^2(\varphi_2^0/\sigma_c^2) \ , \tag{28}$$

$$\beta_0 = (3\varphi_p^0/4\mu)(1 + K_p) \ , \ \beta_1 = (\varphi_1^0/\sigma_c^1)(1 + K_c^1) \ ,$$

$$\beta_2 = (\varphi_2^0/\sigma_c^2)(1 + K_c^2) \ . \tag{29}$$

It is easily demonstrated that Δ is positive if two sets of fractures exist.

SLS model representation of other frequency-dependent terms

There are some other terms in Chapman's (2009) model that are needed to be expressed in terms of the SLS models in addition to H_{ij}^3.

Inserting eq. (20) into eq. (13) and considering eqs. (14) and (15), we can have,

$$H_{ij}^m = y_{0ij}^m + [y_{1ij}^m/(1+i\omega\tau_m)] + [y_{2ij}^m/(1+i\omega\tau_3)] + [y_{3ij}^m/(1+i\omega\tau_4)] \ . \tag{30}$$

Then, substituting eq. (30) into eq. (12), the expression for f_m^p becomes

$$f_m^p = f_{m0}^p + [f_{m1}^p/(1+i\omega\tau_m)] + [f_{m2}^p/(1+i\omega\tau_3)] + [f_{m3}^p/(1+i\omega\tau_4)] \ . \tag{31}$$

And then, the expressions for a_{ij}^m can also be written in the following form,

$$a_{ij}^m = a_{ij}^{m0} + [a_{ij}^{m1}/(1+i\omega\tau_m)] + [a_{ij}^{m2}/(1+i\omega\tau_3)] + [a_{ij}^{m3}/(1+i\omega\tau_4)] \ . \tag{32}$$

To represent C_{ijkl}^p by the SLS model, we consider eqs. (5) and (20), then rewrite p* in the following form,

$$p^* = p^0 + [p^1/(1+i\omega\tau_3)] + [p^2/(1+i\omega\tau_4)] \ . \tag{33}$$

Furthermore, the expression for d in eq. (3) can be written as

$$d = d^0 + [d^1/(1+i\omega\tau_3)] + [d^2/(1+i\omega\tau_4)] \ . \tag{34}$$

Finally, considering eqs. (2) and (34), C_{ijkl}^p can be expressed by the SLS model:

$$C_{ijkl}^p = C_{ijkl}^{p0} + [C_{ijkl}^{p1}/(1+i\omega\tau_3)] + [C_{ijkl}^{p2}/(1+i\omega\tau_4)] \ . \tag{35}$$

Due to page limits, the expressions for y_{kij}^m, f_{mk}^p, a_{ij}^{mk}, p^k, d^k, C_{ijkl}^{pk}, (k = 0,1,2) are not shown in this section.

SLS model representation of C_{ijkl}

According to eqs. (32) and (35) we can represent the frequency-dependent elastic stiffness tensor C_{ijkl} in eq. (1) by the following fourth-order SLS model,

$$C_{ijkl} = M^{ani}_{ijkl} - \sum_{\bar{h}=1}^{4} [M^{\bar{h}}_{ijkl}/(1 + i\omega\tau_{\bar{h}})] \quad , \quad \bar{h} = 1,2,3,4 \quad , \tag{36}$$

It is noted that τ_1 and τ_2 correspond to the relaxation time in eq. (16) for two sets of aligned fractures, respectively. Similarly, τ_3 and τ_4 are the mixed relaxation time for the two sets of aligned fractures in eq. (24). In addition, the other terms in eq. (36) are given below,

$$\begin{aligned}
M^{ani}_{ijkl} &= C^{0}_{ijkl} - C^{p0}_{ijkl} - C^{10}_{ijkl} - C^{20}_{ijkl} \quad , \\
M^{1}_{ijkl} &= C^{11}_{ijkl} \quad , \\
M^{2}_{ijkl} &= C^{21}_{ijkl} \quad , \\
M^{3}_{ijkl} &= C^{p1}_{ijkl} + C^{12}_{ijkl} + C^{22}_{ijkl} \quad , \\
M^{4}_{ijkl} &= C^{p2}_{ijkl} + C^{13}_{ijkl} + C^{23}_{ijkl} \quad ,
\end{aligned} \tag{37}$$

and

$$C^{mn}_{ijkl} = R^{m}_{ip} R^{m}_{jq} R^{m}_{kr} R^{m}_{ls} a^{mn}_{pqrs} \quad , \quad n = 0,1,2,3 \quad . \tag{38}$$

VELOCITY-STRESS CONSTITUTIVE RELATIONSHIP IN THE TIME DOMAIN

In the time-domain staggered grid finite-difference method, the velocity-stress constitutive relationships are needed to simulate the propagation of seismic waves. However, eq. (36) cannot be directly applied to the velocity-stress staggered grid finite-difference method. Here, we derive two types of time-domain velocity-stress formed constitutive relationships by introducing different auxiliary differential equations.

Constitutive Relation A

Based on the effective viscoelastic stiffness tensor in eq. (36), the frequency-domain constitutive relationships can be written in the following form,

$$\tilde{\sigma}_{ij} = M^{ani}_{ijkl}\tilde{\varepsilon}_{kl} - \sum_{\bar{h}=1}^{4} [M^{\bar{h}}_{ijkl}/(1 + i\omega\tau_{\bar{h}})]\tilde{\varepsilon}_{kl} \quad , \tag{39}$$

where $\tilde{\sigma}_{ij}$ denotes stress tensor and $\tilde{\varepsilon}_{kl}$ denotes the strain tensor. The tilde sign denotes frequency-domain.

In order to obtain the time-domain constitutive relationship A, we introduce a memory tensor $\tilde{r}^{\bar{h}}_{ij}$,

$$\tilde{r}^{\bar{h}}_{ij} = -[i\omega M^{\bar{h}}_{ijkl}/(1 + i\omega\tau_{\bar{h}})]\tilde{\varepsilon}_{kl} \quad , \quad \bar{h} = 1,2,3,4 \quad . \tag{40}$$

Consequently, we can obtain the time-domain stress-velocity constitutive relationship A,

$$\partial\sigma_{ij}/\partial t = M^{ani}_{ijkl}(\partial v_k/\partial x_l) + r_{ij} \quad , \tag{41}$$

$$r_{ij} = \sum_{\bar{h}=1}^{4} r^{\bar{h}}_{ij} \quad , \tag{42}$$

$$r^{\bar{h}}_{ij} + \tau_{\bar{h}}(\partial r^{\bar{h}}_{ij}/\partial t) = -M^{\bar{h}}_{ijkl}(\partial v_k/\partial x_l) \quad , \quad \bar{h} = 1,2,3,4 \quad . \tag{43}$$

Constitutive relationship A is similar to that given by Carcione (1995, 1999) for viscoelastic, anisotropic media.

Constitutive Relation B

Besides constitutive relationship A derived above, there is an alternative way to construct the time-domain constructive relationships between the stress and strain tensors, which is called constitutive relationship B. We first rewrite the effective viscoelastic stiffness (36) into the following form:

$$C_{ijkl} = C^{0}_{ijkl} + \sum_{\bar{h}=1}^{4} [i\omega C^{\bar{h}}_{ijkl}/(1 + i\omega\tau_{\bar{h}})] \quad , \tag{44}$$

where,

$$C^{0}_{ijkl} = M^{ani}_{ijkl} - \sum_{\bar{h}=1}^{4} M^{\bar{h}}_{ijkl} \quad , \tag{45}$$

$$C^{\bar{h}}_{ijkl} = \tau_{\bar{h}} M^{\bar{h}}_{ijkl} \quad , \quad \bar{h} = 1,2,3,4 \quad . \tag{46}$$

Introducing auxiliary stress tensors followed by the inverse Fourier transformation, time-domain constitutive relations B can be obtained,

$$\sigma_{ij} = \sum_{\bar{h}=0}^{4} \sigma_{ij}^{\bar{h}} \quad , \tag{47}$$

$$\partial\sigma_{ij}^{0}/\partial t = C_{ijkl}^{0}(\partial v_k/\partial x_l) \quad , \tag{48}$$

$$\sigma_{ij}^{\bar{h}} + \tau_{\bar{h}}(\partial\sigma_{ij}^{\bar{h}}/\partial t) = C_{ijkl}^{\bar{h}}(\partial v_k/\partial x_l) \quad , \quad \bar{h} = 1,2,3,4 \quad , \tag{49}$$

where σ_{ij} denotes the stress tensor, $\sigma_{ij}^{\bar{h}}(\bar{h} = 0,\ldots,4)$ denotes the auxiliary stress tensor, and v_i denotes the i-th component of the particle velocity vector.

Constitutive relationship B is similar to that derived by Dhemaied and Rejiba (2011) for viscoelastic isotropic media through the auxiliary differential equation method.

Therefore, the solution to the wave propagation for Chapman's (2009) model has two types of first-order velocity-stress wave equations in the time domain. The first is to combine constitutive relationship A in eqs. (41) to (43) and velocity-stress formed dynamic equation. The other is to use constitutive relationship B in eqs. (47) to (49) and dynamic equation. Based on one of these, we can design a complete velocity-stress staggered grid finite difference methods to model seismic wave propagation.

NUMERICAL EXPERIMENTS

Comparison of SLS and Chapman's model

To verify the validity of the SLS representation of Chapman's (2009) model, we compare the viscoelastic stiffness predicted by eq. (44) and that directly obtained by Chapman's (2009) model in eq. (1) for a wide range of frequencies.

Here we consider a fractured rock with $v_P = 4$ km/s and $v_S = 2$ km/s, corresponding to the P- and S-wave velocities of the background isotropic medium and the density is 2.2 g/cm^3 and porosity is 1%. The saturated fluid is gas with acoustic velocity of 341 m/s, density of 0.057 g/cm^3 and a viscosity of 1.36×10^{-5} Pa·s. There are two sets of fractures. For the first set of fractures, the radius is 15 m, the volume fraction is 0.1, and the aspect ratio is 0.0001. The first set of fractures is assumed to be along the horizontal plane. For the

second set of fractures, the radius is 10 m, the volume fraction is 0.05, the aspect ratio is 0.0001. The second set of fractures is assumed to be vertical with the normal direction in the y-axis. Moreover, the permeability of the background medium is 1 mD.

We now calculate the effective viscoelastic stiffness variation with frequency using Chapman's (2009) formulas and compare with the SLS formulas derived in this paper. The non-zero viscoelastic stiffness elements are compared in Fig. 1, which indicates that the SLS representation of Chapman's (2009) model is exact at a large frequency range.

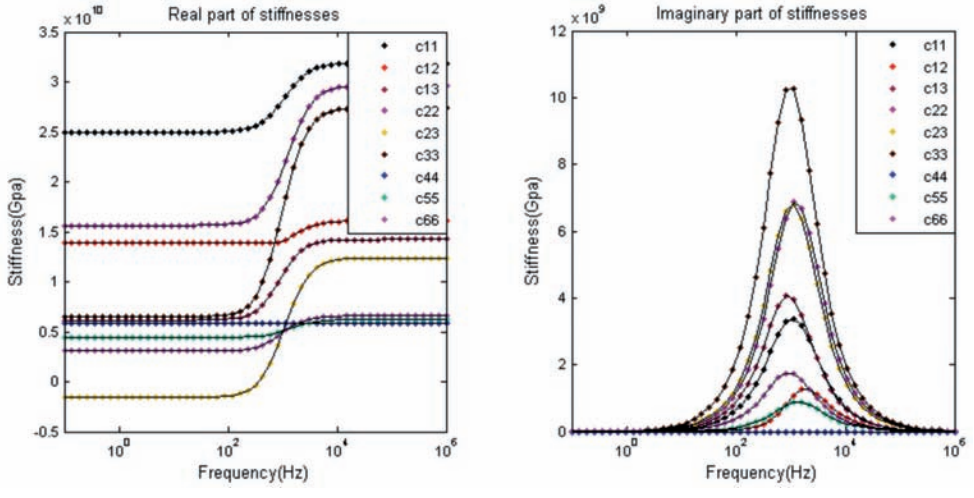

Fig. 1. Comparison of the viscoelastic stiffness calculated by the Chapman's model (black solid lines) and the SLS model (coloured dot line).

Effect of fluid saturation on wave propagation

In this example, we study the fluid saturation on the seismic propagation using numerical modelling of seismic wavefield in the frequency-dependent anisotropic media. Constitutive relationship B proposed in this paper is adopted. According to the velocity-stress wave eqs. (47) to (49), we apply the staggered grid pseudo-spectral method in the following example proposed by Carcione (1999) to simulate wave propagation. First-order spatial derivatives are calculated using the Fourier pseudo-spectral method. The first-order temporal derivatives are approximated by second-order finite-difference.

In Fig. 2, we consider a vertically fractured model with one set of fractures. The model consists of 300 × 300 points with a grid spacing of 10 m. The parameters for the background isotropic medium are the same as that given in the earlier example in Fig. 1. To see the effect of attenuation on seismic waves, porosity is increased to 10%. The fracture radius is 15 m, the volume fraction is 0.1, the aspect ratio is 0.0001. Dipping angle is 90 degrees (i.e., the fractures are vertically assigned), and the azimuthal angle is 45 degrees. The fluid parameters are listed in Table 1. Moreover, the permeability of this model is 1 mD for all three types of fluids.

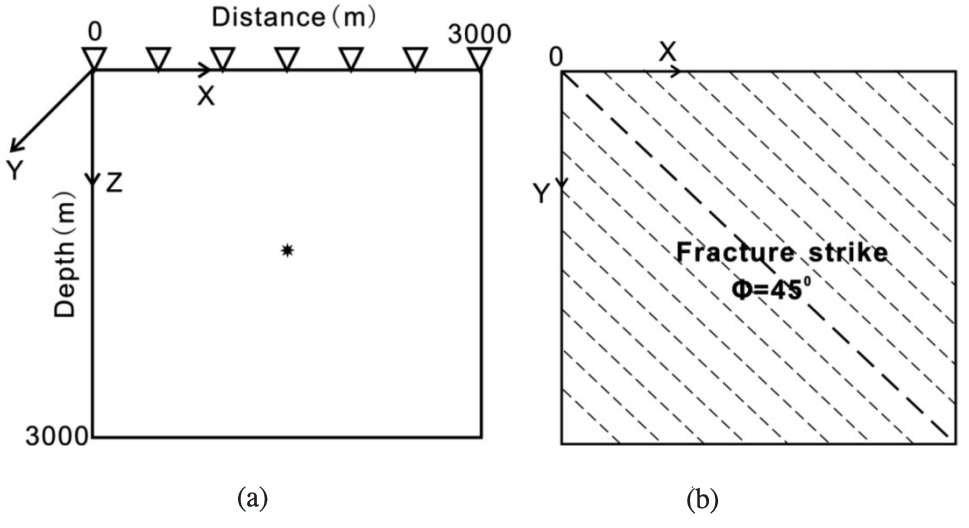

Fig. 2. (a) Homogeneous vertically fractured model with strike angle $\phi = 45°$. (b) A map view of this model.

Table 1. Fluid parameters.

Fluid	Par.	Sonic Velocity (m/s)	Density (kg/m^3)	Bulk modulus (Gpa)	Viscosity (Pa·s)
Oil		1250	800	1.2500	2×10^{-2}
Brine		1527	985	2.2968	4.36×10^{-4}
Gas		341	57	0.0066	1.36×10^{-5}

The time interval is 0.1 ms. A vertical force source is used with a Ricker wavelet of a dominant frequency of 35 Hz as shown in Fig. 3 and the source is placed in the centre of the model.

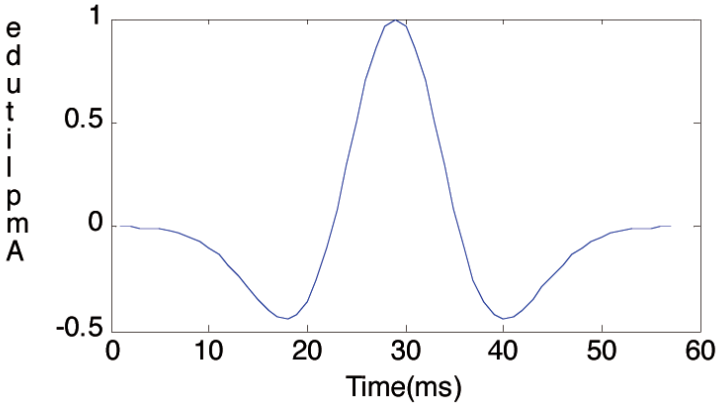

Fig. 3. A Ricker wavelet.

Fig. 4 shows the three velocity components computed for each fluid. A force acting in the z-direction can produce not only x- and z-components but also y-component. Shear-wave splitting is evident for the receivers near the source (near offsets). All nine plots are shown in the same scale in order to compare the amplitude variations. Obviously, the attenuation of seismic waves in gas saturated media is very large. With the increasing in offset, the attenuation becomes clear. However, for the case of oil and brine saturations, the difference is very small.

Fig. 5 shows the three components of particle velocities at Trace no.50. We notice that for the case of gas saturation, the amplitudes of qP-, qS1- and qS2-waves are the smallest among three cases of fluid saturation. The amplitudes for brine saturation model are weaker than the case of oil saturation. We can also notice that the arrival time of qP-wave for the case of brine saturation is earlier than for the case of oil saturation, which means that qP-wave propagates faster in brine saturated fractures than in oil saturated fractures. In contrast, the arrival times of qS1- and qS2-waves for the case of brine saturation is later than for the case of oil saturation, indicating qS1- and qS2-waves propagate in brine saturated fractures in a slower velocity than in oil saturated fractures. Because the amplitudes of qP-, qS1- and qS2-waves propagation in gas saturated fractures are so small that we cannot determine the relationship of arrival time between the cases of gas saturation and the other two cases.

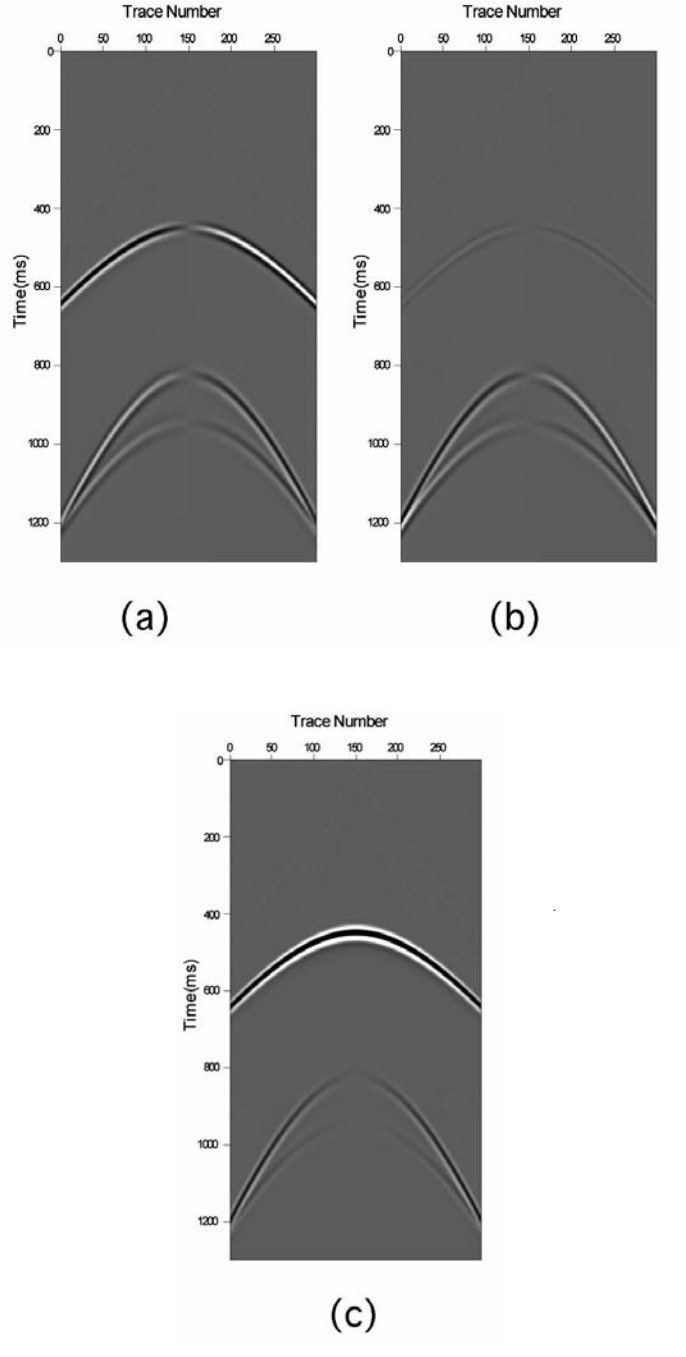

Fig. 4. Three component particle velocities for oil, brine and gas (all plots are displayed in the same scale). The three rows from top to bottom correspond to the cases of oil, brine and gas, respectively. The three columns from left to right correspond to the x-, y- and z-component of particle velocities, respectively.

(a) x-components

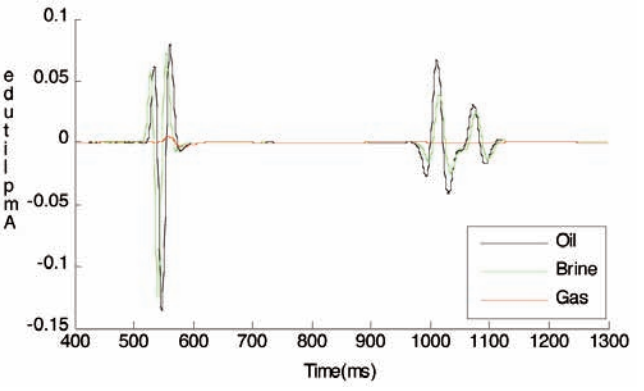

(b) y-components

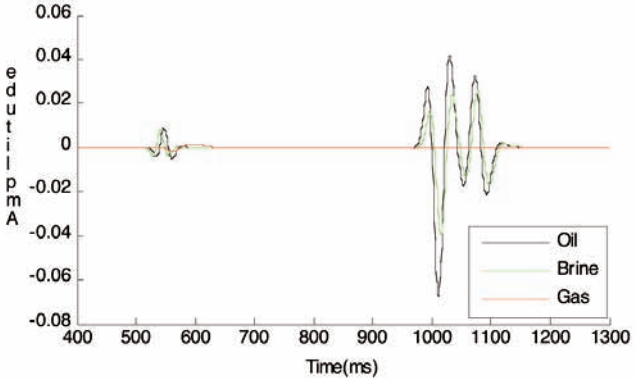

(c) z-components

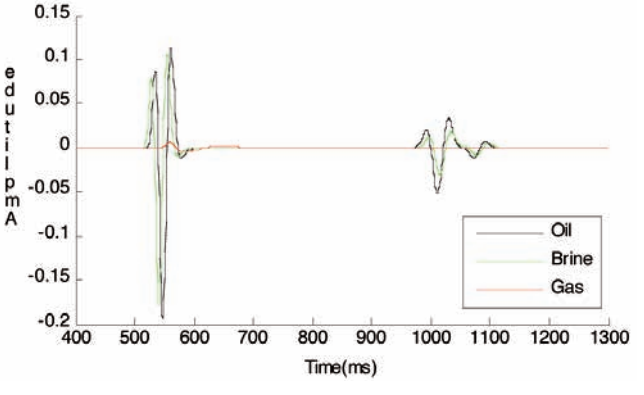

Fig. 5. Particle velocities at trace No. 50.

CONCLUSIONS

Viscoelastic stiffness of Chapman's (2009) model for two sets of aligned fractures can be decomposed into a fourth-order SLS model. By transforming the frequency-domain SLS model into the time-domain, we can obtain two types

of constitutive relationship that can be used in the simulation of seismic wave propagation.

Numerical modelling of wave propagation in homogeneous and vertically fractured media shows that the attenuation of qP-, qS1- and qS2-waves for the case of gas saturation is larger than the other two cases (oil and brine saturations). This phenomenon can be used to qualitatively distinguish fractured gas sandstones from fractured oil and brine sandstones.

ACKNOWLEDGEMENTS

This research work was supported by the grant from China University of Petroleum (Grant No. 11CX04002A). We are grateful to Dr. Enru Liu (ExxonMobil Upstream Research Company) for his comment on this work. The first author also thanks Abraham Ho for his help to improve the English.

REFERENCES

Al-Harrasi, H.O., Kendall, J.M. and Chapman, M., 2011. Fracture characterization using frequency-dependent shear wave anisotropy analysis of microseismic data. Geophys. J. Internat., 185: 1059-1070.

Carcione, J.M., 1995. Constitutive model and wave equations for linear, viscoelastic, anisotropic media. Geophysics, 60: 537-548.

Carcione, J.M., 1999. Staggered mesh for the anisotropic and viscoelastic wave equation. Geophysics, 64: 1863-1866.

Chapman, M., 2003. Frequency-dependent anisotropy due to meso-scale fractures in the presence of equant porosity. Geophys. Prosp., 51: 369-379.

Chapman, M., 2009. Modelling the effect of multiple sets of mesoscale fractures in porous rock on frequency dependent anisotropy. Geophysics, 74: D97-D103.

Dhemaied, A. and Rejiba, F., 2011. Seismic-wave propagation modelling in viscoelastic media using the auxiliary differential equation method. Bull. Seismol. Soc. Am., 101: 413-420.

Liu, E., Maultzsch, S., Chapman, M., Li, X.Y., Queen, J.H. and Zhang, Z.J., 2003a. Frequency-dependent seismic anisotropy and its implication for estimating fracture size in low porosity reservoirs. The Leading Edge, 22: 662-665.

Liu, E., Queen, J.H., Li, X.Y., Chapman, M., Maultzsch, S., Lynn, H.B. and Chesnokov, E.M., 2003b. Observation and analysis of frequency-dependent anisotropy from a multicomponent VSP at Bluebell-Altamont Field, Utah. J. Appl. Geophys., 54: 319-333.

Liu, E., 2005. Effects of fracture aperture and roughness on mechanical and hydraulic properties of rocks, implication of seismic fracture characterization. J. Geophys. Engin., 2: 38-47.

Liu, E., Chapman, M., Zhang, Z.J. and Queen, J.H., 2006. Frequency-dependent anisotropy: effects of multiple fracture sets on shear-wave polarizations. Wave Motion, 44: 44-57.

Maultzsch, S., Chapman, M., Liu, E. and X.Y., Li,, 2003. Modelling frequency-dependent seismic anisotropy in fluid-saturated rock with aligned fracture: implication of fracture size estimation from anisotropic measurements. Geophys. Prosp., 51: 381-392.

Maultzsch, S., Chapman, M., Liu, E. and Li, X.Y., 2007. Modelling and analysis of attenuation anisotropy in multi-azimuth VSP data from the Clair field. Geophys. Prosp., 55: 627-642.

Tillotson, P., Chapman, M., Best, A.I., Sothcott, J., McCann, C., Wang, S. and Li, X.Y., 2011. Observations of fluid-dependent shear-wave splitting in synthetic porous rocks with aligned penny-shaped fractures. Geophys. Prosp., 59: 111-119.